A Hirshfeld surface analysis, crystal structure and spectroscopic properties of new Zn(II) complex with N-aminoethylpiperazine ligand

Maroua El Glaoui, Maher El Glaoui, Christian Jelsch, Emmanuel Aubert, Frederic Lefebvre, Cherif Ben Nasr

Published in *Journal of Molecular Structure*, 2017, *1134*, 538-545.

doi.org/10.1016/j.molstruc.2017.01.015

A Hirshfeld Surface Analysis, Crystal Structure and spectroscopic properties of new Zn(II) complex with N-aminoethylpiperazine ligand

Maroua El Glaoui[a], Maher El Glaoui[b], Christian Jelsch[c], Emmanuel Aubert[c], Frédéric Lefebvre[d], Chérif Ben Nasr[a]*

[a] Laboratoire de Chimie des Matériaux, Faculté des Sciences de Bizerte, 7021 Zarzouna, Tunisia.

[b] Laboratoire de Valorisation des Matériaux Utiles, Centre National des Recherches en Sciences des Matériaux (CNRSM), Technopôle de Borj-Cédria, 8027 Soliman, Tunisia.

[c] CRM^2, CNRS, Institut Jean Barriol, Université de Lorraine, Vandoeuvre les Nancy, France.

[d] Laboratoire de Chimie Organométallique de Surface (LCOMS), Ecole Supérieure de Chimie Physique Electronique, 69626 Villeurbanne Cedex, France.

Abstract

A new organic-inorganic hybrid material, 1-amonioethylpiperazine-1, 4-diium tetrachloridozincate(II) chloride, $(C_6H_{18}N_3)[ZnCl_4]Cl$, has been synthesized and characterized by various physicochemical techniques including UV-visible absorption, Infra-Red (IR), Raman and NMR spectroscopies. The compound crystallizes in the monoclinic system and $P2_1$ space group with $Z = 2$ and the following unit cell dimensions: $a = 7.1728$ (6), $b = 12.4160$ (11), $c = 8.0278$ (7) Å, $\beta = 97.513$ (1)°, $V = 708.80$ (11) Å^3.

In this structure, the Zn^{2+} ion, surrounded by four chlorides, adopts a distorted tetrahedral coordination geometry. The structure of this compound consists of monomeric 1-amonioethylpiperazine-1, 4-diium trications and monomeric $[ZnCl_4]^{2-}$ and Cl^- anions. These entities are interconnected by means of hydrogen bonding contacts [N-H…Cl, C-H…Cl],

forming a three-dimensional network. Intermolecular interactions were investigated by Hirshfeld surfaces. More than three quarters of the interaction surface in the crystal packing is constituted by attractive and favored H…Cl hydrogen bonds. The ^{13}C and ^{15}N CP–MAS NMR spectra are discussed and the vibrational absorption bands were identified by infrared and Raman spectroscopy.

Keywords: Zn(II) complex; X-ray diffraction; NMR spectroscopy, Ultraviolet-visible (UV–vis) spectroscopy, Hirshfeld surface analysis, Coordination compound.

Introduction

In recent years, there has been an increasing interest in organic-inorganic compounds, whose combination may convey the synergy properties of both moieties into one hybrid compound. This enables them to exhibit some interesting crystal structures and properties such as second-order nonlinear optical (NLO) response, magnetic, electronic, conductivity, luminescence and ferroelectric properties [1 - 9]. Additionally investigation of the Zn(II) frameworks in terms of photoluminescence was thoroughly performed recently [10, 11]. Moreover, in organic-inorganic hybrid metal halides, hydrogen bonds play an important role in stabilizing the frameworks of the cations and their counter inorganic species. The energy of N-H… hydrogen bonds and their possible role in supramolecular chemistry continue to attach much attention [12].

Therefore, in this paper we present the synthesis, structural and spectral characterization of $(C_6H_{18}N_3)[ZnCl_4]Cl$.

1. Experimental

1.1. Synthesis

The organic-inorganic hybrid compound, $(C_6H_{18}N_3)[ZnCl_4]Cl$, was prepared by reaction of *N*-aminoethylpiperazine, $C_6H_{15}N_3$, and Zinc chloride. First, $ZnCl_2$ (1 mmol; 0.17 g) was added to an *N*-aminoethylpiperazine (1 mmol; 0.19 g) solution dissolved in 15 mL of absolute ethanol. The resulting solution was then acidified with 1 mL of concentrated HCl and allowed to evaporate slowly at room temperature. Colorless block like crystals of $(C_6H_{18}N_3)[ZnCl_4]Cl$ were formed after two weeks (yield, 87.7%).

The reactions sequence for the synthesis is shown in the following equation:

$$C_6H_{15}N_3 + ZnCl_2 + 3\ HCl \rightarrow (C_6H_{18}N_3)[ZnCl_4]Cl$$

1.2. Crystal structure determination

Single crystals were carefully selected under a microscope and mounted on a Mitegen micromesh with the help of a trace of mineral oil. X-ray diffraction data were collected at 100 K on a Bruker AXS SMART APEX CCD diffractometer using the ω scan technique with MoKα radiation (λ = 0.7107 Å). Diffraction data were collected, the unit cell determined, and the data integrated and corrected for absorption and other systematic errors using the APEX2 suite of programs [13]. SHELXS-97 [14] was used to solve the structure using direct methods and SHELTXL6.14 [15], SHELXL2013 [16] and SHELXLE [17] were used for refinement.

The drawings were made with Diamond [18]. The final anisotropic full-matrix least squares resulted in a convergence of the R factor at 0.015, R_w = 0.037. Crystal data and experimental parameters used for the intensity data collection are summarized in Table 1.

1.3. IR spectroscopy

The IR spectra were recorded in the range 4000 - 400 cm^{-1} with a ‘‘Perkin-Elmer FTIR’’ spectrophotometer 1000 using samples dispersed in spectroscopically pure KBr pressed into a pellet.

1.4. Raman measurements

For Raman measurements, a good transparent single crystal of $(C_6H_{18}N_3)[ZnCl_4]Cl$ was selected and the Raman scattering spectrum was performed using HORIBA Scientific spectrometer (lab. RAM HR) equipped with Laser source (632 nm) and CCD detector with standard attachment in the frequency range 100 - 3500 cm^{-1} at room temperature.

1.5. Electronic spectrum

The electronic spectrum was recorded on a Perkin-Elmer Lambda 950 spectrophotometer within the range 200 - 800 nm.

2. Results and discussions

2.1. Structure description

The asymmetric unit of the title compound is formed by one 1-amonioethylpiperazine-1, 4-diium trication, one tetrachlorozincate dianion and one isolated chloride anion (Fig. 1).

In the structural arrangement, the inorganic ions, $ZnCl_4^{2-}$, NH_3^+, NH_2^+ and Cl^-, are interconnected through N-H···Cl hydrogen bonds to form layers parallel to the (**a**, **b**) plane (Fig. S1) and located at z = ½ (Fig. 2).

The organic group and the free Cl^- anions are interconnected via N-H…Cl and C-H…Cl hydrogen bonds to form layers parallel to the (**b**, **c**) plane (Fig. S2). These layers, situated at x = 0 (Fig. S3), are interconnected by the $ZnCl_4^{2-}$ anions via N-H…Cl and C-H…Cl hydrogen bonds to form the crystal packing (Fig. S4).

The complex $[ZnCl_4]^{2-}$ anion is distorted due to its involvement in hydrogen-bonding interactions. The $[ZnCl_4]^{2-}$ and Cl^- anions are well separated by Van der Waals contacts and consequently there is no basis for describing the Zn(II) species as a distorted $[ZnCl_5]^{3-}$ anion.

3.1.1. Geometry and coordination of the tetrachlorozincate dianion

The geometry of $ZnCl_4$ verifies the reported relation (Table 2). The Zn-Cl distances vary between 2.2582 (4) and 2.2813 (5) Å with a mean value of 2.268 Å. The Cl-Zn-Cl angle values are in the 104.667 (16) - 112.083 (16)° range with a mean value of 109.494° and indicate relatively little distortion from a regular tetrahedron. Taking into account the geometrical characteristics of the entities and considering the calculated average values of the Baur distortion indices (*DI*) deduced from the following formula [19]:

$$DI(Zn-Cl) = \sum_{i=1}^{n_1} \frac{|d_i - d_m|}{n_1 d_m}$$

$$DI(Cl-Zn-Cl)=\sum_{i=1}^{n_2}\frac{|a_i-a_m|}{n_2 a_m}$$

Where d_m is the mean value for (Zn-Cl) distances and a_m the mean value for (Cl-Zn-Cl) angles. *DI* (Zn-Cl) = $3.8.10^{-3}$, *DI* (Cl-Zn-Cl) = 0.025, with n_1 = 4 and n_2= 6.

The low values of these indices are possibly due to the fact that all chlorine atoms are involved in weak hydrogen bonds.

3.1.2. Geometry and coordination of the organic cation

The organic group is located in the (**b**, **c**) plane (Fig. S2). Table 2 reports the main geometrical features of the $[C_6H_{18}N_3]^{3+}$ cations. The C-N bond lengths vary from 1.488(2) to 1.507(2) Å. The C-C bond lengths vary from 1.514 (2) to 1.515 (2) Å. These values are in agreement with those found in related compounds [20].

The conformation of the piperazine-diium six-membered ring can be described in terms of Cremer and Pople puckering coordinates [21], i.e., evaluating the parameters *Q* (total puckering amplitude), q_2, q_3, θ and φ. The calculated values for N1-C1-C2-N3-C4-C6 ring are as follows: *Q* = 0.565 Å, q_2 = 0.0094 Å, q_3 = -0.565 Å, θ = 179.04° and φ = -78.12° corresponding to the structure of the most stable chair conformation.

2.2. Vibrational studies

The FTIR and Raman spectra of crystalline $(C_6H_{18}N_3)[ZnCl_4]Cl$ are displayed in Figs. S5 and S6 respectively and the vibrational assignments are listed in Table 4.

The comparison of the IR spectrum of the title compound with that of the pure amine (Fig. S5) shows, in particular, that the presence of the tetrachlorozincate anion shifts the bands related to the NH_2 and NH groups of the amine, situated at 3382 and 3287 cm^{-1}, at lower

wavenumbers, between 3121 and 3078 cm^{-1}. This shift towards the low frequencies is attributed to the formation of hydrogen bonds N-H…Cl in the salt.

The most representative and characteristic vibrational modes of this compound can be compared to those of similar compounds [22 - 29]. The asymmetric and symmetric modes of NH_3 stretching vibration are observed at 3121 and 3078 cm^{-1} in FTIR. N-H and C-H asymmetric stretching vibrations are assigned to the peaks observed at 2982 cm^{-1} in FTIR, while the peak at 2447 cm^{-1} in IR is assigned to N-H and C-H symmetric stretching vibrations. The peaks found at 1570 and 1507 cm^{-1} in FTIR and at 1574, 1557, 1500 and 1482 cm^{-1} in Raman are assigned to NH_2 wagging and CH_2 scissoring vibrations. Considering the CH_2 group vibrations, the deformation of CH_2 and N-H deformation are observed at 1470 and 1445 cm^{-1} in FTIR, respectively and at 1470 and 1440 cm^{-1} in Raman. The peaks at 1396 and 1335 cm^{-1} in IR are assigned to CH_2 wagging vibrations and are observed at 1402, 1394, 1334 and 1312 cm^{-1} in Raman. The CH_2 and NH_2 twisting vibrations modes are found at 1286 cm^{-1} in FTIR and 1290, 1281 and 1214 cm^{-1} in Raman. The observed peaks at 1181, 1151, 1077 and 1048 cm^{-1} in FTIR and in Raman at 1192, 1147, 1046 and 1036 cm^{-1} correspond to CH_2 rocking and C-C stretching vibrations. (C-C), (N-H) and (C-N) stretching, (C-N-H) bending and CH_3 rocking are identified in the strip area located between 1006 and 747 cm^{-1} in IR and between 1003 and 744 cm^{-1} in Raman. Further, the peak that appeared at 622 cm^{-1} in IR and the peaks between 620 and 387 cm^{-1} in Raman are assigned to the C-N-C and C-C-N deformation. The low frequency Raman absorption peaks occurring at 299, 282, 123 and 110 cm^{-1} are due to internal vibrations of $ZnCl_4^{2-}$ ion.

The calculated IR spectrum between 500 and 4000 cm^{-1} is shown in Fig. S7 and is very similar to the experimental one. A close agreement between the experimental and calculated wave numbers is mostly achieved in the fingerprint region as shown in Fig. S8. Thus, the

precision is well-sufficient to assign the experimental frequencies and to confirm the attributions proposed above.

2.3. UV-visible spectroscopy

Fig. S9 shows the experimental UV-Vis absorption spectrum of $(C_6H_{18}N_3)[ZnCl_4]Cl$ at room temperature. As seen, there are three distinct absorption peaks at 225, 285 and 385 nm, which are very comparable to those found in other materials previously reported containing organic-inorganic hybrid compound, such as $(C_8H_{10}NO)_2[CdCl_4]$ [30], $(C_{10}H_{21}NH_3)[CuCl_4]$ [31], $(C_7H_8N_3)[CdI_4]$ [32]. The nethermost energy absorption peaks at 385 nm is caused by band gap absorption and it is attributed to the excitation of free electron-hole pairs within the $[ZnCl_4]^{2-}$ inorganic chain. This peak is mostly due to a photo-induced exciton constituted by the transition from the top of the valence band including of Cl(3p) orbital to the bottom of the Zn(4s) conduction band (absorption between Cl(3p) and Zn(4s) (band to band)). This suggests that the compound behaves as semiconductor material and is compatible with the color of the crystal. The bands with maximum energies at 225 and 285 nm can be assigned to the absorption of a highest energetic level in the conduction band.

2.4. Hirshfeld surface and contacts enrichment ratios

The Hirshfeld surface of the title compound was generated using Crystal Explorer [33]. The Hirshfeld surface is used to identify the intermolecular interactions including H…Cl, H…H, Cl…Cl contacts. Three-dimensional (3D) Hirshfeld surface maps are generated with d_{norm} using a red-white-blue color scheme, indicating shorter contacts, Van der Waals contacts, and longer contacts, respectively, and the decomposed two dimensional fingerprint plots generated using d_e and d_i distances lead to analyze all of the intermolecular contacts and to summarize the nature and type of all intermolecular contacts in the crystal structure.

The enrichment ratios [34] of contacts between the different chemical species were computed in order to highlight which contacts are favored and are likely to be the crystal driving force.

The Hirshfeld surface was computed around the independent organic cation, one $ZnCl_4$ anion, and one chloride anion (Fig. 3 (a, b and c)). The intensive red hot spots on the surface colored according to d_{norm} correspond to hydrogen bonds with neighboring molecules. The 2D fingerprint plots can be decomposed to highlight a particular atom pair close contacts and to enable the separation of contributions from different interactions of each subgroup of the asymmetric unit (Fig. S10, S11 and S12).

Globally the H and Cl chemical types constitute the large majority (46 and 47%) of the Hirshfeld surface on the three ions present the asymmetric unit. The organic cation surface is covered by 95% of hydrogen which mostly interacts with chloride atoms, as can be seen in Fig. 4. The intermolecular H…Cl contacts are predominant as they constitute more than three quarters of the total interaction surface (Table 5). The hydrogen atoms (Hn, Hc) bound to N and C are distinguished in Table 5, as their electrostatic properties are different. The Hc…Cl contacts, which are weak hydrogen bonds, constitute nearly half of the contact surface. The strong H-bonds Hn…Cl^- are more enriched (E=2.0) than the weaker Hc…Cl^- interactions (E=1.6). There are indeed ten N-H…Cl and ten C-H…Cl hydrogen bonds in the crystal structure (Table 3, Fig. S10). The Hn…Cl and, to a lesser extent, the Hc…Cl contacts are electrostatically favorable due to the complementary partial charges δ^+ of H and δ^- of chloride atoms.

The Zn…Hc contacts are the most enriched (E=2.3) but constitute only 5.4% of contacts; they are presumably a consequence of their proximity with the large proportion of Zn…Cl^- contacts. All self-contacts, including the hydrophobic interaction Hc…Hc are significantly avoided with low E<0.45 values. Chloride and hydrogen atoms constitute both nearly one half of the Hirshfeld surface; as consequence there is a good surface

complementarity between H-bond acceptors and donors while hydrophobic contacts (mainly Hc…Hc) between organic cations represent only 5% of the contact surface. In summary, the crystal packing is essentially maintained by attractive and favored strong Hn…Cl^- and weak Hc…Cl^- hydrogen bonds.

2.5. Quantum mechanical study

Quantum chemical calculation was performed from the crystal data with DFT method at the 6-311++G(d,p) basis set, by using the Gaussian 09 program. Fig. 5 clearly shows that the highest occupied orbital (HOMO) is mainly localized on the CH_2 groups, while the lowest unoccupied orbital (LUMO) is mainly localized on the N-H groups. The large HOMO-LUMO gap of 10.2 eV implies high kinetic stability and low chemical reactivity [35, 36], because it is energetically unfavorable to add electrons to a high-lying LUMO or to extract electrons from a low-lying HOMO [37].

Beside these isolated molecule computations, periodic DFT calculations were also undertaken using the Castep 8.0 software [38]. Starting with the experimental X-ray structure geometry, positions of all atoms were optimized while keeping the unit cell parameters fixed to the corresponding experimental values. The PBE functional was selected, completed with Grimme dispersion correction [39]; on-the-fly ultrasoft pseudopotentials were used, and a plane wave cutoff of 600 eV was selected and tested for geometry convergence, together with a k-point spacing of 0.03 $Å^{-1}$ leading to 26 points for the sampling of the Brillouin zone. The resulting optimized structure is very close to the experimental one as shown by the superposition of the two (Fig. 6), the major differences being the positions of hydrogen atoms, which are too close to their covalently bonded C, N heavy atoms in the X-ray structure, as expected.

2.6. NMR results

The ^{13}C CP-MAS NMR spectrum of $(C_6H_{18}N_3)[ZnCl_4]Cl$ is shown in Fig. S13. It exhibits six well-resolved resonances corresponding to the six crystallographically independent carbon atoms. This is in agreement with only one organic molecule being present in the asymmetric unit cell as revealed by the X-ray structure determination.

The ^{15}N CP-MAS NMR spectrum of the title compound (Fig. S14) is also in good agreement with the X-ray structure. Indeed, it exhibits well-defined signals with an intensity ratio of 1:2 at -361.9 and -358.1 ppm corresponding to the three crystallographic independent nitrogen atoms, in agreement with only one organic molecule in the asymmetric part of the unit cell.

Density functional theory (DFT) calculations were undertaken in order to assign the NMR resonances to the different crystallographic non-equivalent carbon and nitrogen atoms of the unit cell. These calculations were made at the B3LYP/6-311++G** level. The different atoms were labeled as depicted below:

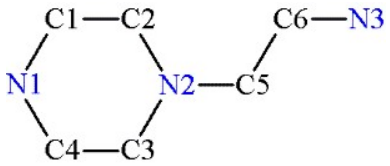

The calculations were made on the organic cation after optimization of the position of the protons and the theoretical chemical shifts were subtracted from those of the reference (tetramethylsilane for carbon with δ_{exp} = 0 ppm and glycine for nitrogen with δ_{exp} = -347.2 ppm and δ_{th} = -238.0 ppm) calculated at the same level of theory.

The results are listed on Table 6 and Fig. 7. Clearly, there is a very good agreement between the experimental and the theoretical values calculated after optimization of the position of the protons, allowing unambiguously the attribution of the different NMR signals, even

though some calculated values for the isotropic chemical shifts are far away from the experimental ones.

It is worth noticing that the discrepancy between the calculated and experimental values is mainly due to the fact that an isolated molecule was taken into account. A better agreement was then obtained by computing the isotropic part of the NMR shielding tensors by periodic DFT calculations using the Castep 8.0 software. Indeed, the coefficient of determination in the linear regression analysis with respect to the experimental values rose to 0.9996 (as compared to 0.9643 for the isolated molecule calculation).

Concluding remarks

We have developed new $(C_6H_{18}N_3)[ZnCl_4]Cl$ crystals, which show the monoclinic space group $P2_1$ with a minimal tetrahedral distortion of the $[ZnCl_4]^{2-}$ ion. In the structure, the different inorganic ions are interconnected through N-H···Cl hydrogen bonds to form layers parallel to the (**a**, **b**) plane. The piperazinediium six-membered ring adopts the most stable chair conformation. The crystal structure is stabilized via the various types of hydrogen bonding interactions, N-H···Cl and C-H···Cl. The Hirshfeld surface analysis reveals that the intermolecular H…Cl contacts are predominant. NMR signals are in full agreement with the crystallographic data. DFT calculations allow the attribution of the experimental NMR lines and of IR bands at low frequencies.

Supplementary data

Crystallographic data for the structural analysis have been deposited at the Cambridge Crystallographic Data Centre, CCDC No 1509981. These data can be obtained free of charge via http://www.ccdc.cam.ac.uk/conts/retrieving.html, or from the CCDC, 12 Union Road, Cambridge, CB2 1EZ, UK: fax: (+44) 01223-336-033; e-mail: deposit@ccdc.cam.ac.

Acknowledgment

Thanks to Professor Matthias Zeller of Youngstown State University (USA) for his fruitful collaboration. The diffractometer was funded by NSF grat 0087120, by Ohio Board of Reagents grant CAP-491, and by YSU. This work was granted access to the HPC resources of TGCC/CINES/IDRIS under the allocation 2017-A0010807449 made by GENCI.

References

[1] M. Zdanowska-Fraczek, K. Holderna-Natkaniec, Z. J. Fraczek, R. Jakubas, Molecular dynamics and electrical conductivity of $(C_3N_2H_5)_5Bi_2Cl_{11}$, Solid. State Ion 180 (2009) 9 - 12.

[2] I. Chaabane, F. Hlel, K. Guidara, Electrical study by impedance spectroscopy of the new compound $[C_{12}H_{17}N_2]_2CdCl_4$, J. Alloys Compd. 461 (2008) 495 - 500.

[3] K.-I. Sakai, M. Takemura, Y. Kawabe, Lead chloride-based layered perovskite incorporated with an excited state intramolecular proton transfer dye, J. Lumin. 130 (2010) 2505 - 2507.

[4] K. Pradeesh, G. SharachandarYadav, M. Singh, G. Vijaya Prakash, Synthesis, structure and optical studies of inorganic-organic hybrid semiconductor, $NH_3(CH_2)_{12}NH_3PbI_4$, Mater. Chem. Phys. 124 (2010) 44 - 47.

[5] A. K. Vishwakarma, P. S. Ghalsasi, A. Navamoney, Y. Lan, A. K. Powell, Structural phase transition and magnetic properties of layered organic-inorganic hybrid compounds: p-Haloanilinium tetrachlorocuparate(II), Polyhedron 30 (2011) 1565 - 1570.

[6] C. Aruta, F. Licci, A. Zappettini, F. Bolzoni, F. Rastelli, P. Ferro, T. Besagni, Growth and optical, magnetic and transport properties of $(C_4H_9NH_3)_2MCl_4$ organic-inorganic hybrid films (M= Cu, Sn), Appl. Phys. A81 (2005) 963 - 968.

[7] M. Bujak, J. Zaleski, High temperature ferro-paraelectric phase transition in tris (trimethylammonium) nonachlorodiantimonate(III) (TMACA) studied by X-ray diffraction method, Cryst. Eng. 4 (2001) 241 - 252.

[8] K. Karoui, A. Ben Rhaiem, K. Guidara, Dielectric properties and relaxation behavior of $[TMA]_2Zn_{0.5}Cu_{0.5}Cl_4$ compound, Phys. B407 (2012) 489 - 493.

[9] B. Kulicka, T. Lis, V. Kinzhybalo, R. Jakubas, A. Piecha, Novel anionic water-containing inorganic fragment in $[4\text{-}NH_2PyH]_8[Bi_2Cl_{11}][Bi_2Cl_9(H_2O)_2]$: Structural characterization, thermal, dielectric and vibrational properties, Polyhedron 29 (2010) 2014 - 2022.

[10] S. Konar, A. Jana, K. Das, S. Ray, S. Chatterjee, J. A. Golen, A. L. Rheingold, S. K. Kar, Synthesis, crystal structure, spectroscopic and photoluminescence studies of manganese(II), cobalt(II), cadmium(II), zinc(II) and copper(II) complexes with a pyrazole derived Schiff base ligand, Polyhedron 30 (2011) 2801 - 2808.

[11] C.-X. Ding, C.-H. He, Y.-S. Xie, Syntheses and structures of tetranuclear Zn(II) complexes with in situ generated macrocyclic Schiff base ligands: Applications in Zn^{2+} sensing, Chin. Chem. Lett. 24 (2013) 463 - 466.

[12] L. Brammer, J. K. Swearingen, E. A. Bruton, P. Sherwood, Hydrogen bonding and perhalometallate ions: A supramolecular synthetic strategy for new inorganic materials, Proc. Natl. Acad. Sci. USA 99 (2002) 4956 - 4961.

[13] Bruker Apex2, Advanced X-ray Solutions Bruker AXS Inc., Madison, Wisconsin, USA (2009).

[14] G. M. Sheldrick, A short history of SHELX, Acta Cryst. A64 (2008) 112 - 122.

[15] Bruker Advanced X-ray Solutions, SHELXTL (Version 6.14), Bruker AXS Inc., Madison, Wisconsin, USA, (2003).

[16] G. M. Sheldrick, SHELXL2013, University of Göttingen, Germany (2013).

[17] C. B. Hübschle, G. M. Sheldrick, B. Dittrich, ShelXle: a Qt graphical user interface for SHELXL, J. Appl. Cryst. 44 (2011) 1281 - 1284.

[18] K. Brandenburg, Diamond Version 2.0 Impact GbR, Bonn., Germany (1998).

[19] W. H. Baur, The geometry of polyhedral distortions. Predictive relationships for the phosphate group, Acta Cryst. B30 (1974) 1195 - 1215.

[20] F. Issaoui, I. Baccar, E. Dhahri, O. El Sadek, F. Zouari, E. K. Hlil, Synthesis, Crystal Structure, Magnetism, Band Structure and Density of States of $[C_6H_{18}N_3]ClCoCl_4$, J. Supercond. Nov. Magn. 25 (2012) 1563 - 1570.

[21] D. Cremer, J. A. Pople, A General Definition of Ring Puckering Coordinates, J. Am. Chem. Soc. 97 (1975) 1354 - 1358.

[22] A. Kessentini, M. Belhouchet, J. J. Suñol, Y. Abid, T. Mhiri, Crystal structure, vibrational studies and optical properties of a new organic-inorganic hybrid compound $(C_{10}H_{28}N_4)CuCl_5Cl{\cdot}4H_2O$, Spectrochim. Acta, Part A: Mol. Biomol. Spectrosc. 134 (2015) 28 - 33.

[23] S. Kalyanaraman, V. Krishnakumar, H. Hagemann, K. Ganesan, Infrared and polarized Raman spectra of dixanthinium tetrachlorozincate single crystal, J. Phys. Chem. Solids 68 (2007) 256 - 263.

[24] R. Priya, S. Krishnan, G. Bhagavannarayana, S. Jerome Das, Growth and characterization of novel ferroelectric bis(methylammonium) tetrachlorozincate, Physica B 406 (2011) 1345 - 1350.

[25] S. Krishnan, C. Justin Raj, S. Dinakaran, R. Uthrakumar, R. Robert, S. Jerome Das, Optical, thermal, dielectric and ferroelectric behaviour of sodium acid phthalate (SAP) single crystals, J. Phys. Chem. Solids 69 (2008) 2883 - 2887.

[26] William T. A. Harrison, Ethylenediaminium tetrachlorozincate, Acta Cryst. E61 (2005) m1951 - m1952.

[27] K. Nakamoto, Infrared and Raman Spectra of Inorganic Coordination Compounds, Wiley-Interscience, NewYork, 1978.

[28] S. Gunasekaran, B. Anita, Spectral investigation and normal coordinate analysis of piperazine, Indian J. Pure Appl. Phys. 46 (2008) 833 - 838.

[29] J. Orive, E. S. Larrea, R. Fernández de Luis, M. Iglesias, J. L. Mesa, T. Rojo, M. I. Arriortua, Amine templated open-framework vanadium(III) phosphites with catalytic properties, Dalton Trans. 42 (2013) 4500 - 4512.

[30] A. Jellibi, I. Chaabane, K. Guidara, Spectroscopic ellipsometry and UV-vis studies at room temperature of the novel organic-inorganic hybrid of salt Bis (4-acetylanilinium) tetrachlorocadmiate, Physica E79 (2016) 167 - 172.

[31] W. Wang, X. Chen, S. Efrima, Silver Nanoparticles Capped by Long-Chain Unsaturated Carboxylates, J. Phys. Chem. B 103 (1999) 7238 - 7246.

[32] A. Kessentini, M. Belhouchet, J. J. Suñol, Y. Abid, T. Mhiri, Synthesis, crystal structure, vibrational spectra, optical properties and theoretical investigation of bis (2-aminobenzimidazolium) tetraiodocadmate, J. Mol. Struct. 1039 (2013) 207 - 213.

[33] S. K. Wolff, D. J. Grimwood, J. J. McKinnon, M. J. Turner, D. Jayatilaka, M. A. Spackman, CRYSTAL-EXPLORER 3.0, The University of Western Australia, (2012).

[34] C. Jelsch, S. Soudani, C. Ben Nasr, Likelihood of atom-atom contacts in crystal structures of halogenated organic compounds, IUCr J. 2 (2015) 327 - 340.

[35] S. K. Seth, S. Banerjee, T. Kar, Crystal structure and DFT calculations of andrographiside, J. Mol. Struct. 965 (2010) 45 - 49.

[36] S. K. Seth, N. C. Saha, S. Ghosh, T. Kar, Structural elucidation and electronic properties of two pyrazole derivatives: A combined X-ray, Hirshfeld surface analyses and quantum mechanical study, Chem. Phys. Lett. 506 (2011) 309 - 314.

[37] Z. L. Wang, L. H. Wei, L. Y. Jin, J. P. Wang, Synthesis, Structure and Theoretical Calculation of Imidazolium 3, 5-Dinitrobenzoate, Chin. J. Struct. Chem. 26 (2007) 1423 - 1428.

[38] S. J. Clark, M. D. Segall, C. J. Pickard, P. J. Hasnip, M. J. Probert, K. Refson, M. C. Payne, First principles methods using CASTEP, Z. Kristallogr. 220 (2005) 567 - 570.

[39] S. Grimme, Semiempirical GGA-type density functional constructed with a long-range dispersion correction, J. Comput. Chem. 27 (2006) 1787 - 1799.

Figures

Fig. 1

A view of the asymmetric unit in the crystal structure of the title compound showing the atom-numbering scheme and displacement ellipsoids drawn at the 50% probability level. The dotted lines indicate hydrogen bonds.

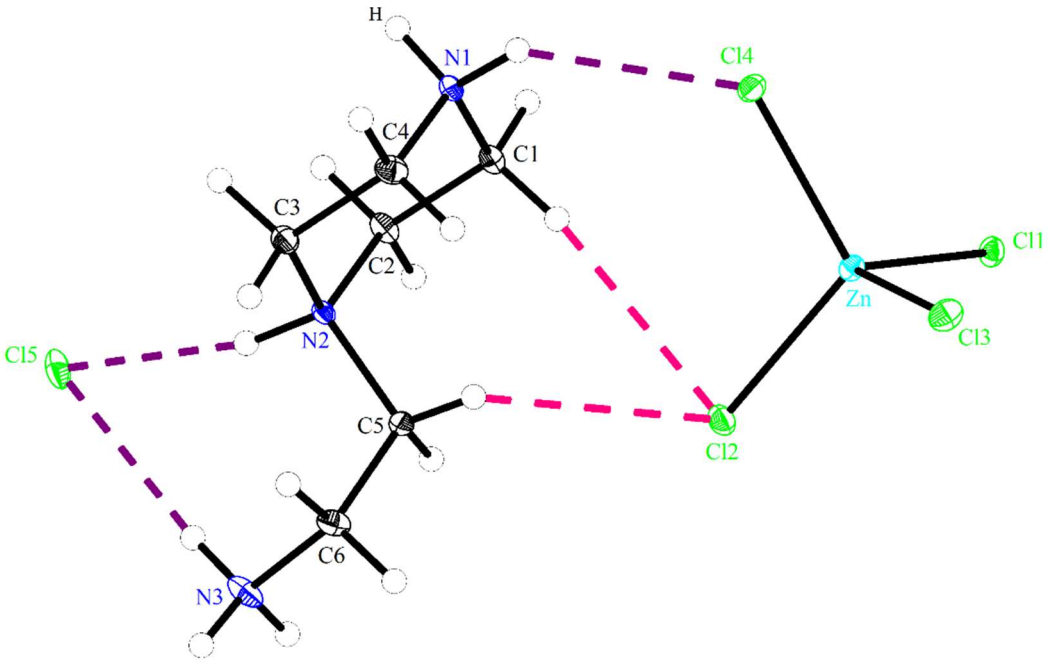

Fig. 2 Projection of a layer situated at z = ½ of the crystal structure of $(C_6H_{18}N_3)[ZnCl_4]Cl$ in the (**a**, **c**) plane. The dotted lines indicate hydrogen bonds.

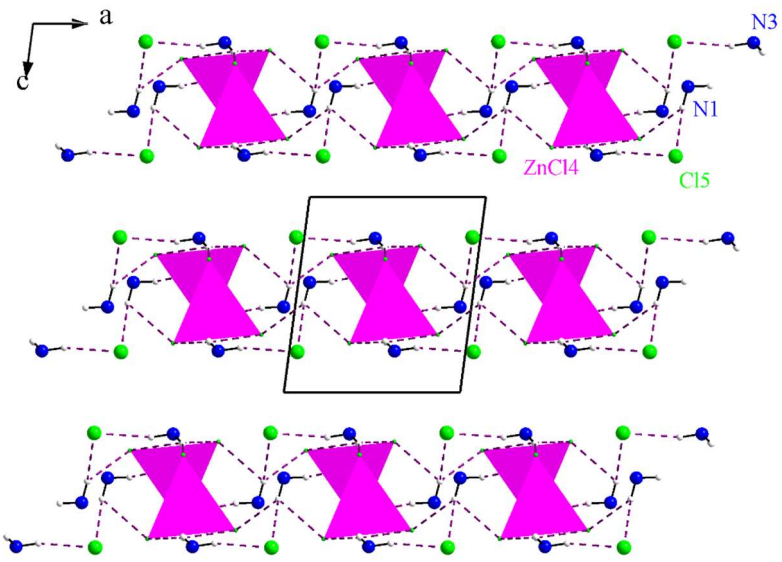

Fig. 3

Hirshfeld surfaces mapped around the cation (a), the $ZnCl_4$ (b) and Cl^- moieties (c) with d_{norm}, the surface is shown as transparent to allow visualization of the orientation of subgroups of the asymmetric unit.

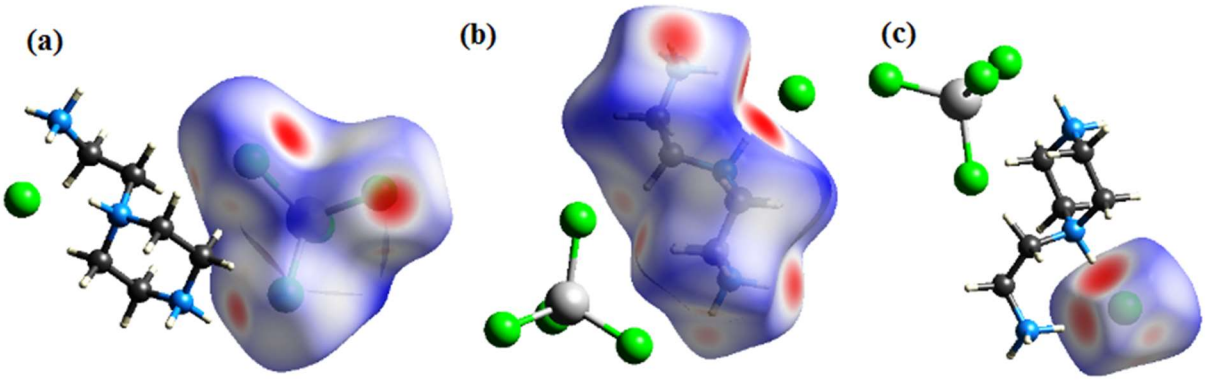

Fig. 4 Hirshfeld surface around the three independent moieties in the crystal.

(a) Colored according to the interior atom contributing most to the electron density

(b) exterior atom.

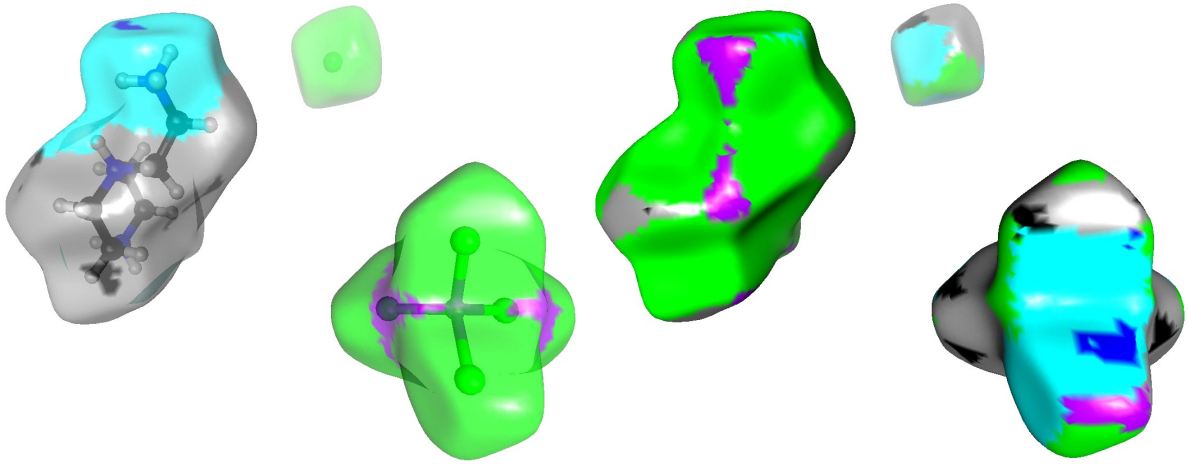

(a) (b)

Fig. 5

Frontier molecular orbitals (HOMO and LUMO) of $(C_6H_{18}N_3)[ZnCl_4]Cl$.

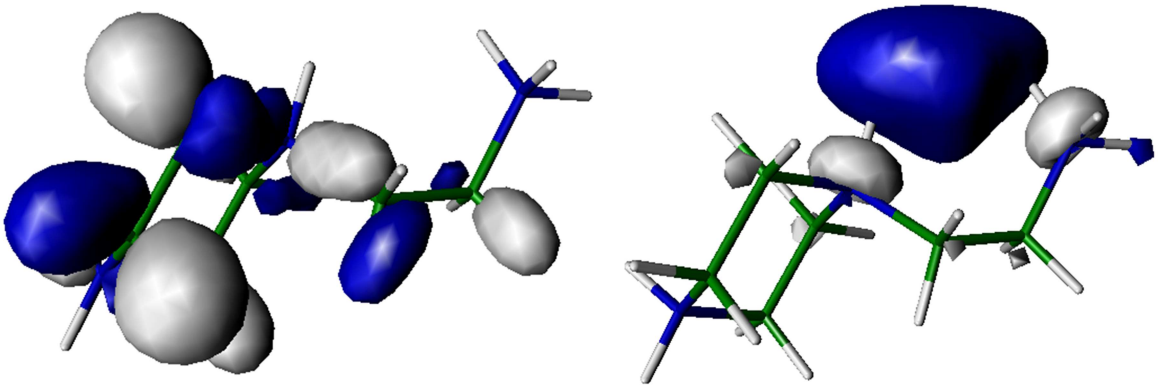

E(HOMO) = -22.80 eV

E(LUMO) = -12,60 eV

Fig. 6 Superposition of the experimental and optimized structures of the title compound.

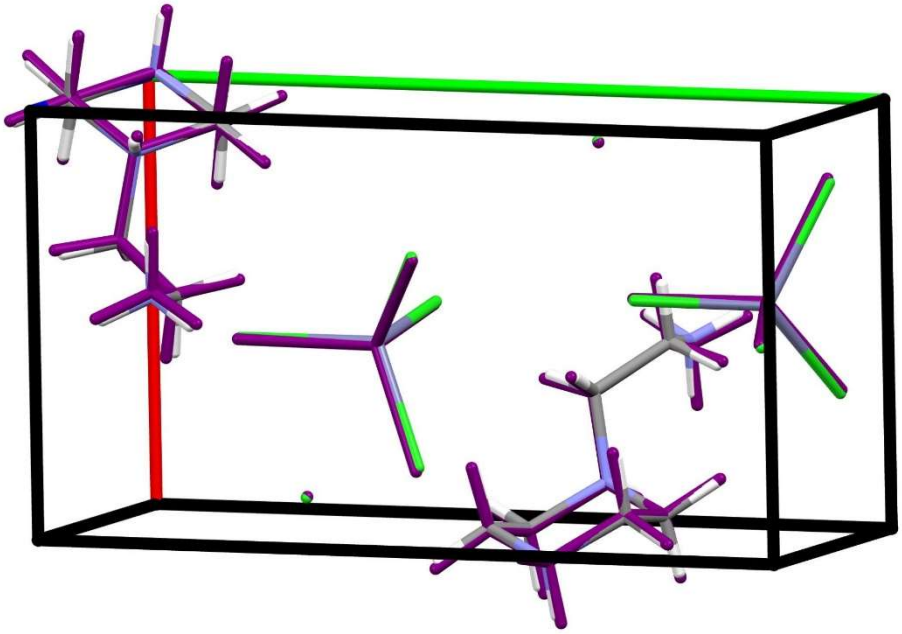

Fig. 7

Comparison between experimental and calculated chemical shifts in $(C_6H_{18}N_3)[ZnCl_4]Cl$.

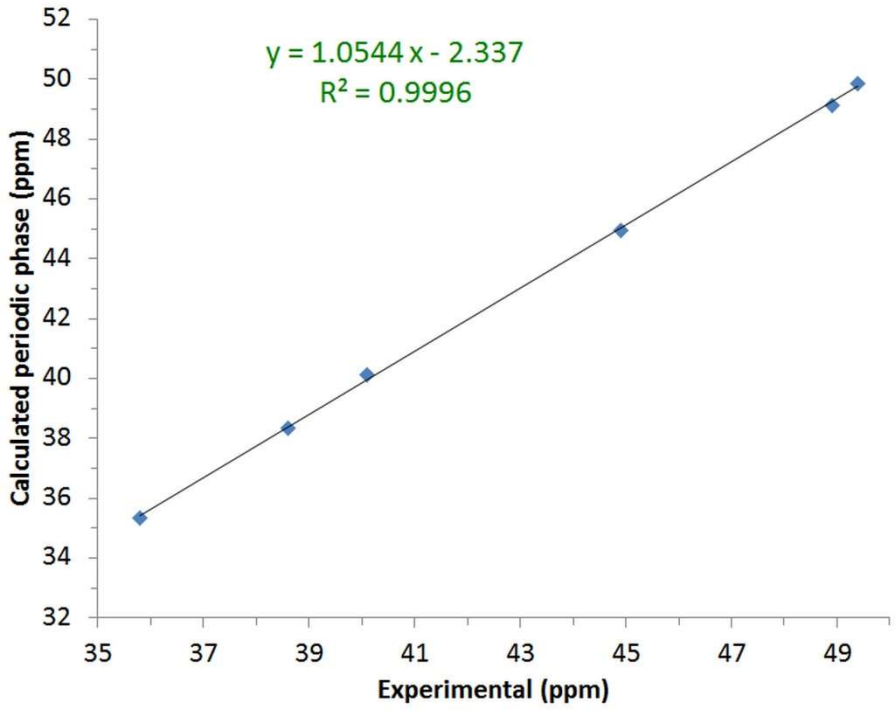

Table 1 Crystal data and structure refinement parameters of $(C_6H_{18}N_3)[ZnCl_4]Cl$.

Formula	$(C_6H_{18}N_3)[ZnCl_4]Cl$
Molecular weight ($g.mol^{-1}$)	374.85
μ (Mo$K\alpha$) (mm^{-1})	2.65
Temperature (K)	100
Crystal system / space group	Monoclinic / $P2_1$
a (Å)	7.1728 (6)
b (Å)	12.4160 (11)
c (Å)	8.0278 (7)
β (°)	97.513 (1)
V (Å^3)	708.80 (11)
Z	2
D_x (Mg m^{-3})	1.756
Crystal size (mm^3)	0.58 × 0.46 × 0.34
Crystal colour / shape	Colorless / Block
hkl range	$-10 \leq h \leq 10$ $-18 \leq k \leq 18$ $-11 \leq l \leq 11$
θ range for data collection (°)	2.6 - 32.2
Diffractometer	Bruker AXS SMART APEX CCD
Refinement method	Full-matrix least-squares on F^2
Programs system	SHELXS97 and SHELXL2013
Absorption correction	Multi-scan Apex2 v2014.11 (Bruker, 2014)
No. of measured, independent and observed [$I > 2\sigma(I)$] reflections T_{min} = 0.486, T_{max} = 0.746	16186, 4535, 4490
# Reflexions numbers / # variables	4535 / 139
No. of restraints	1
R_{int}	0.029
$(\sin\theta/\lambda)_{max}$ ($Å^{-1}$)	0.750
F(000)	380
R indices	$R[F^2 > 2\sigma(F^2)] = 0.015$, $wR(F^2) = 0.037$
Goodness-of-fit on F^2	0.97
Highest peak / deepest hole (e $Å^{-3}$)	$-0.30 \leq \Delta\rho \leq 0.52$
Extinction coefficient: 0.0138 (12)	$(\Delta/\sigma)_{max} = 0.001$
Absolute structure parameter	0.026 (6)

Table 2 Main interatomic distances (Å) and angles (°) of $(C_6H_{18}N_3)[ZnCl_4]Cl$.

Zn1-Cl1	2.2813 (5)	Zn1-Cl3	2.2606 (4)
Zn1-Cl2	2.2721 (5)	Zn1-Cl4	2.2582 (4)
Cl4-Zn1-Cl3	106.056 (17)	Cl4-Zn1-Cl1	111.702 (16)
Cl4-Zn1-Cl2	112.083 (16)	Cl3-Zn1-Cl1	111.103 (17)
Cl3-Zn1-Cl2	111.354 (17)	Cl2-Zn1-Cl1	104.667 (16)
N1-C4	1.496 (2)	N2-C2	1.507 (2)
N1-C1	1.498 (2)	N3-C6	1.488 (2)
C1-C2	1.514 (2)	C3-C4	1.514 (2)
N2-C3	1.504 (2)	C5-C6	1.515 (2)
N2-C5	1.505 (2)		
C4-N1-C1	111.65 (13)	N2-C2-C1	111.88 (13)
N1-C1-C2	110.25 (14)	N2-C3-C4	112.30 (13)
C3-N2-C5	114.44 (13)	N1-C4-C3	110.59 (13)
C3-N2-C2	109.47 (13)	N2-C5-C6	113.70 (13)
C5-N2-C2	112.24 (13)	N3-C6-C5	112.03 (14)

Table 3 Bond length (Å) and angles (°) in the hydrogen bonding scheme of $(C_6H_{18}N_3)[ZnCl_4]Cl$.

D*-H···*A	***D*-H**	**H···*A***	***D*···*A***	***D*-H···*A***
N1-H1*C*···Cl3^{i}	0.91	2.82	3.3514 (15)	119
N1-H1*C*···Cl4	0.91	2.58	3.3064 (15)	138
N1-H1*C*···Cl5^{ii}	0.91	2.74	3.3455 (16)	125
N1-H1*D*···Cl1^{iii}	0.91	2.37	3.2121 (15)	154
C1-H1*A*···Cl2	0.99	2.86	3.8412 (18)	170
C1-H1*B*···Cl2^{i}	0.99	2.93	3.5334 (18)	120
C1-H1B···Cl5^{iv}	0.99	2.92	3.4662 (19)	116
N2-H2···Cl5	1.00	2.07	3.0045 (14)	155
C2-H2*A*···Cl2^{i}	0.99	2.90	3.5959 (17)	128
N3-H3*C*···Cl5	0.91	2.38	3.2594 (17)	163
N3-H3*D*···Cl1^{v}	0.91	2.85	3.2742 (15)	110
N3-H3*D*···Cl2^{v}	0.91	2.32	3.1420 (16)	150
N3-H3*E*···Cl3^{vi}	0.91	2.48	3.3202 (17)	153
N3-H3*E*···Cl4^{vi}	0.91	2.94	3.3641 (16)	110
C3-H3*B*···Cl1^{iii}	0.99	2.81	3.5839 (17)	135
C4-H4*A*···Cl5^{ii}	0.99	2.76	3.3248 (17)	117
C4-H4*B*···Cl1^{vii}	0.99	2.68	3.6372 (17)	164
C5-H5*A*···Cl1^{vii}	0.99	2.77	3.5630 (17)	138
C5-H5*A*···Cl2	0.99	2.74	3.4752 (16)	132
C5-H5*B*···Cl4^{vi}	0.99	2.93	3.6047 (17)	126

Symmetry codes: (i) $x+1, y, z$; (ii) $x, y, z+1$; (iii) $-x+2, y+½, -z+1$; (iv) $-x+2, y-½, -z$; (v) $-x+1, y+½, -z$; (vi) $x, y, z-1$; (vii) $-x+1, y+½, -z+1$.

Table 4 Observed and calculated frequencies (cm^{-1}) of $(C_6H_{18}N_3)[ZnCl_4]Cl$.

Wavenumber FTIR (cm^{-1})	Raman (cm^{-1})	Assignements
3121 3078		NH_3 asymmetric and symmetric stretching
2982 2447		NH_2,(N-H) and (C-H) stretching
1570 1507	1574 1557 1500 1482	NH_2 wagging and CH_2 scissoring
1470	1470	(CH_2) deformation
1445	1440	(N-H) deformation
1396 1335	1402 1394 1334 1312	CH_2 wagging
1286	1290 1281 1214	NH_2 and CH_2 twisting
1181 1151 1077 1048	1192 1147 1046 1036	CH_2 rockingand (C-C) stretching
1006 979 947 899 850 747	1003 978 944 896 866 848 820 744	(C-C), (N-H) and (C-N) stretching + CH_3 rockingand (C-N-H) bending
622	620 519 484 420 387	(C-N-C) and (C-C-N) deformation
	299 282 124 123 110	Internal vibrations of $ZnCl_4^{2-}$

Table 5 Chemical proportions on the Hirshfeld surface of the three entities: organic cation, $ZnCl_4^{2-}$ anion and chloride anion. Actual contacts and their enrichment in the crystal of the title compound are also given (C and N atoms omitted).

atom	Cl	Hn	Hc	Zn	C	N
% surface	46.2	15.3	32.3	3.7	2.2	0.2
Contacts %	Cl	Hn	Hc	Zn		
Cl	6.7					
H	28.3	0.03				
Hc	47.9	0.5	4.4			
Zn	0.9	1.2	5.4	0.0		
Enrichment	Cl	Hn	Hc	Zn		
Cl	0.30					
Hn	1.98	0.01				
Hc	1.61	0.05	0.45			
Zn	0.25	1.08	2.26	0.00		

Table 6 Comparison of calculated and experimental chemical shift values of carbon and nitrogen atoms in the title compound.

Atoms	**Calculated (ppm)**		**Experimental (ppm)**
	Gas phase	**Periodic phase**	
C1	41.8	38.3	38.6
C2	49.1	44.9	44.9
C3	56.9	49.8	49.4
C4	43.2	40.1	40.1
C5	53.6	49.1	48.9
C6	40.6	35.3	35.8
N1	-310	-363	-358
N2	-302.5	-355	-358
N3	-324.5	-359	-362

Supplementary Materials

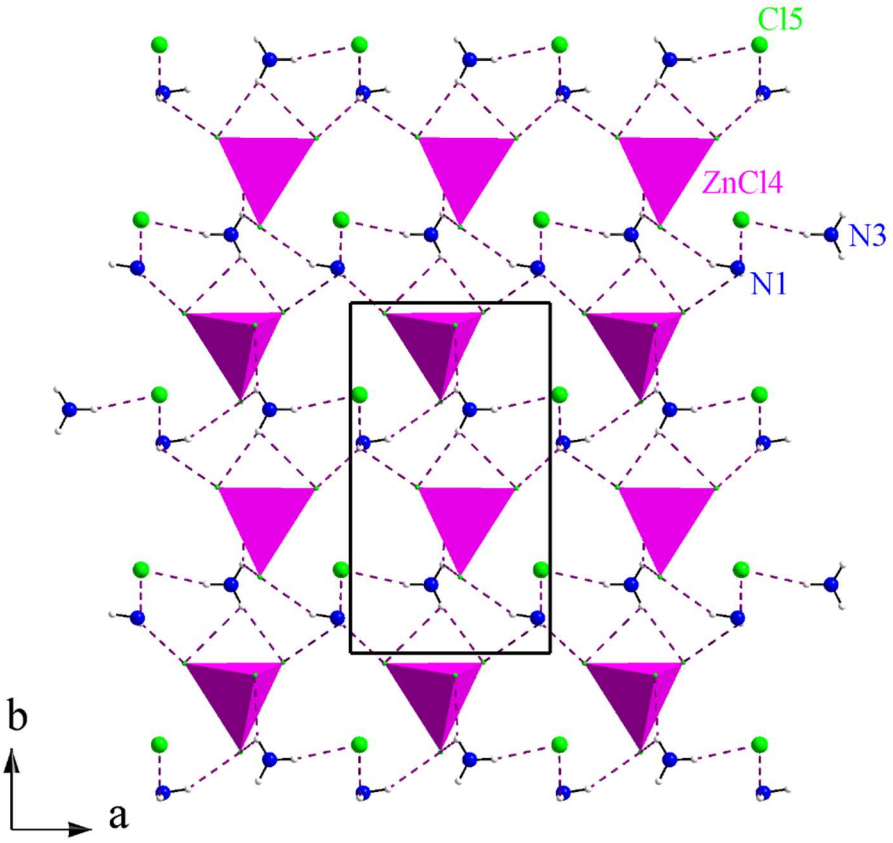

Fig. S1

Projection, along the **a**-axis, of a layer in the inorganic structure of the title compound. The dotted lines indicate hydrogen bonds.

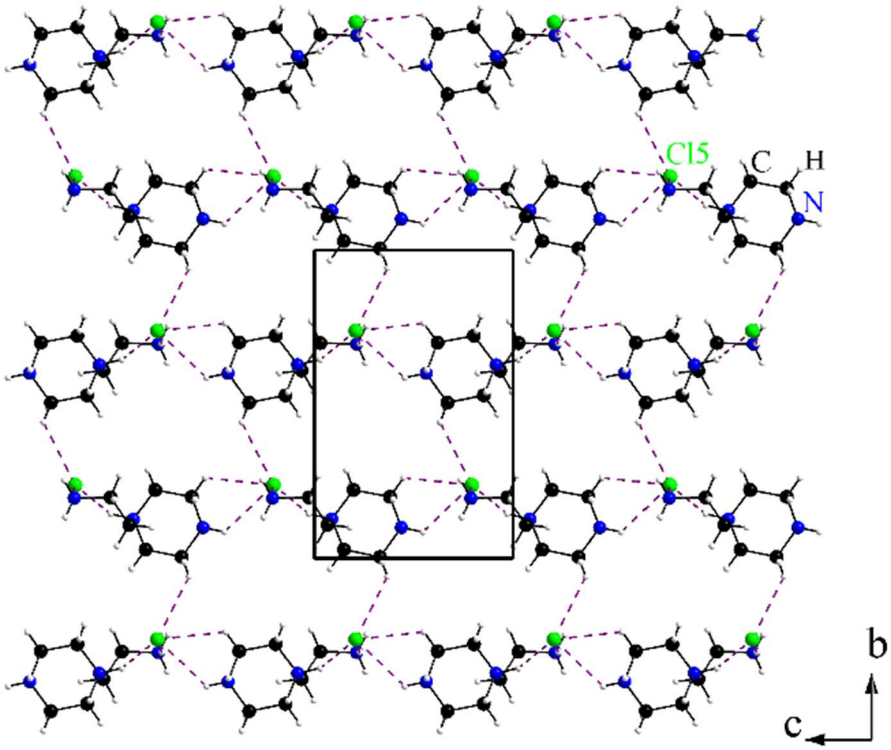

Fig. S2

Projection, along the **c**-axis, of a layer in the structure of the title compound. The dotted lines indicate hydrogen bonds.

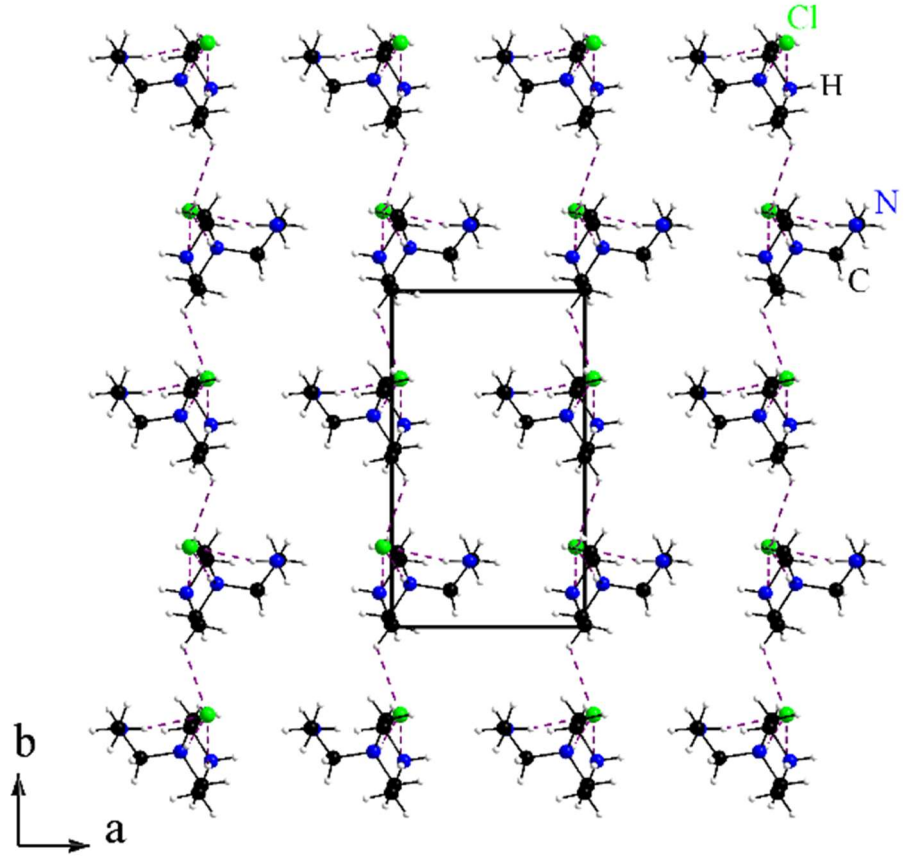

Fig. S3

Projection of a layer situated at x =0 of the crystal structure of $(C_6H_{18}N_3)[ZnCl_4]Cl$ in the (**b**, **c**) plane. The dotted lines indicate hydrogen bonds.

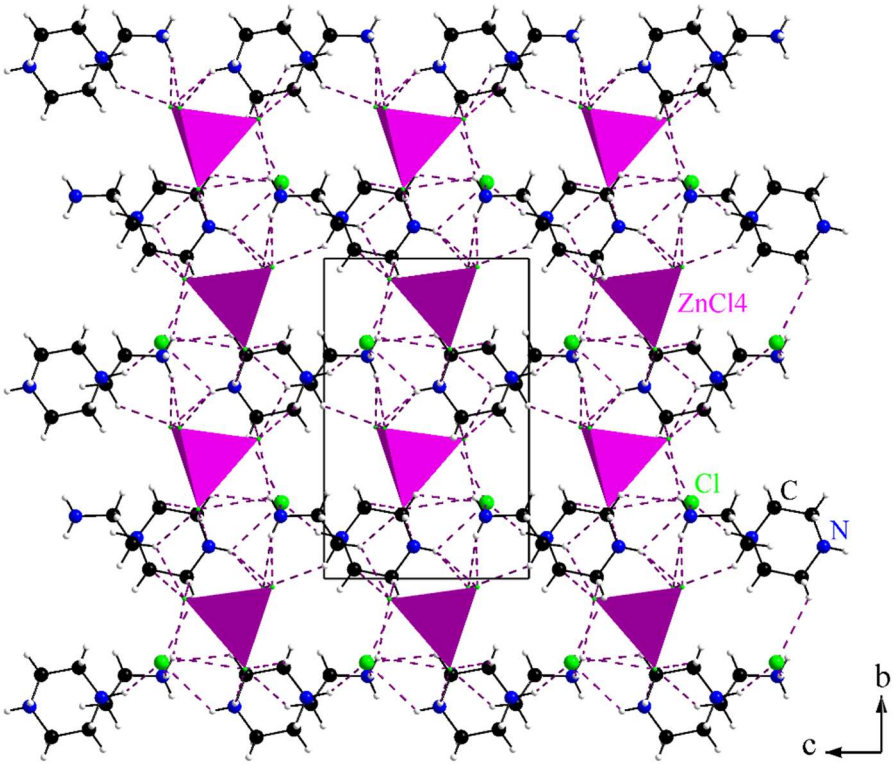

Fig. S4

Projection of the crystal structure of $(C_6H_{18}N_3)[ZnCl_4]Cl$ in the (**b**, **c**) plane, with hydrogen bonds indicated as dashed lines.

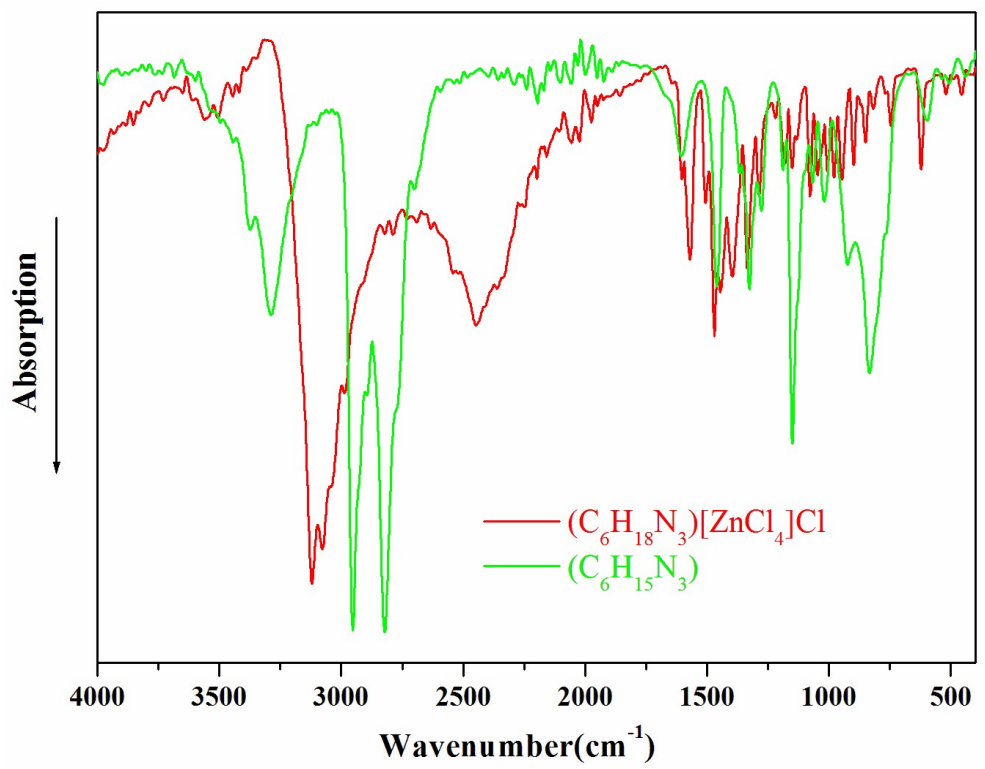

Fig. S5

Infrared spectra of $(C_6H_{18}N_3)[ZnCl_4]Cl$ and the pure amine $(C_6H_{15}N_3)$ in the 400 - 4000 cm^{-1} wavenumber region measured at room temperature.

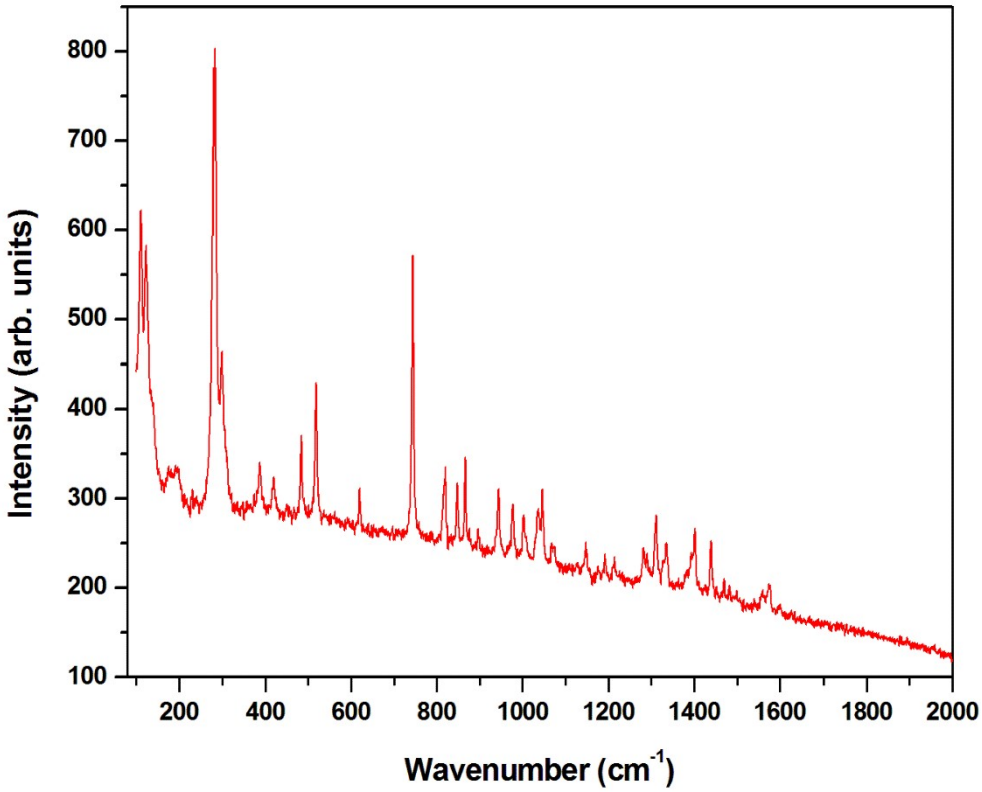

Fig. S6

Raman spectra of $(C_6H_{18}N_3)[ZnCl_4]Cl$ in the 100 - 2000 cm^{-1} wavenumber region measured at room temperature.

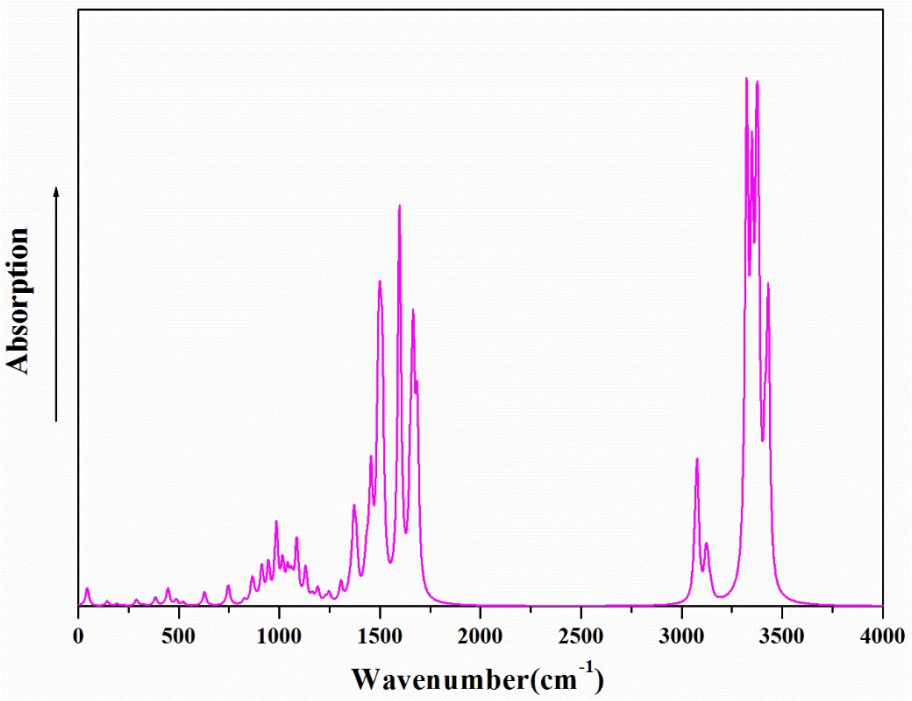

Fig. S7 Calculated IR absorption spectrum of $(C_6H_{18}N_3)[ZnCl_4]Cl$.

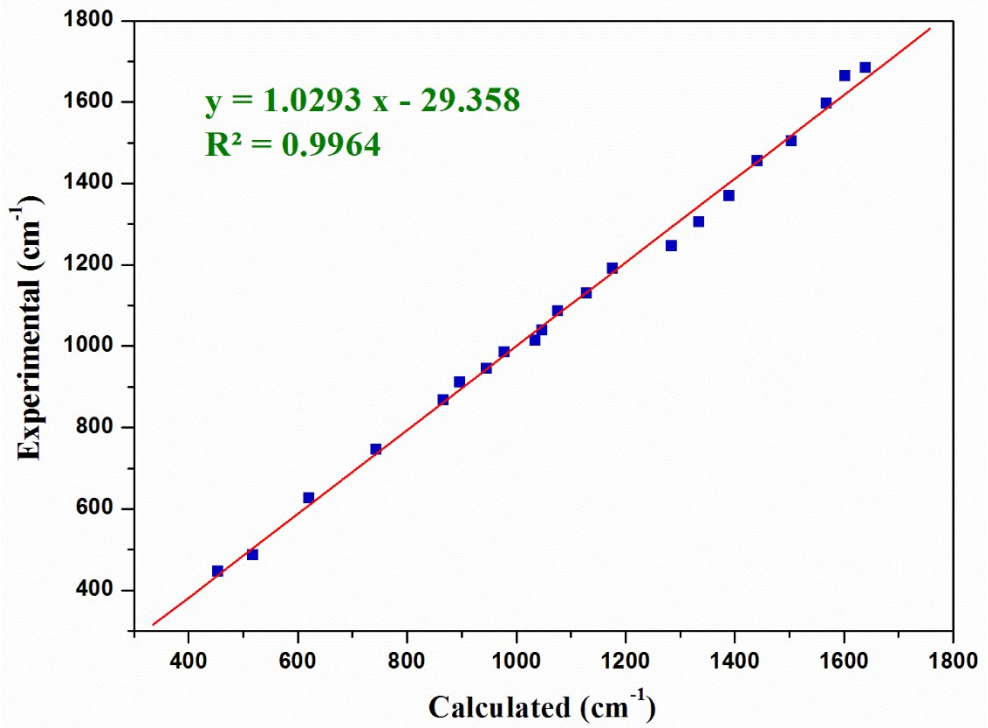

Fig. S8 Comparison between experimental and calculated frequencies of $(C_6H_{18}N_3)[ZnCl_4]Cl$.

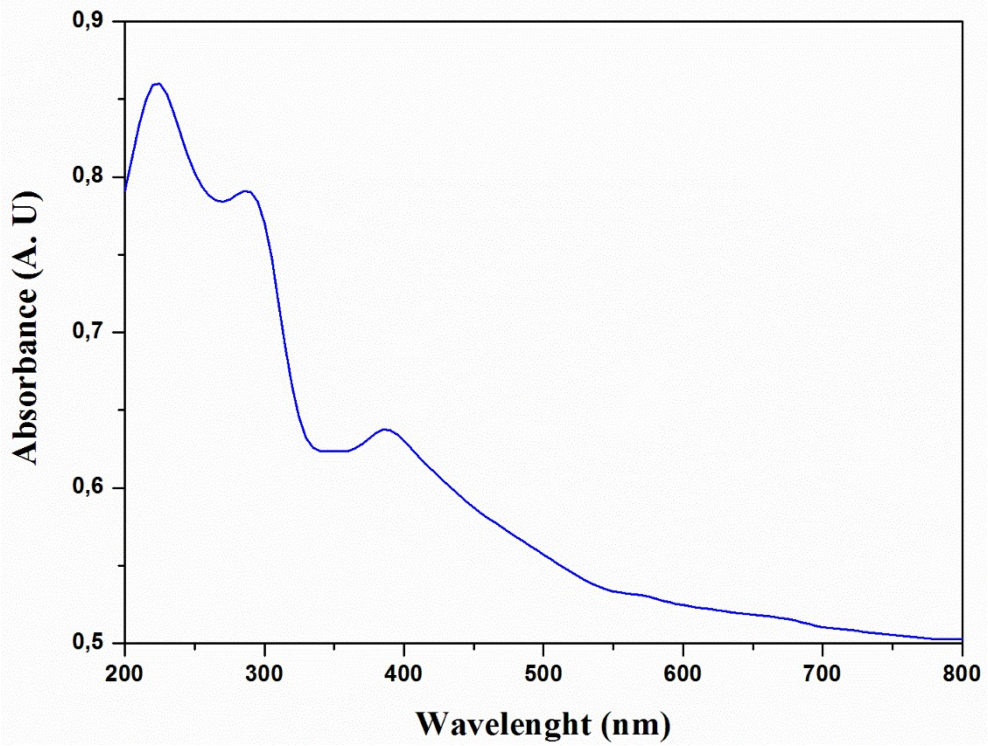

Fig. S9 Variation of the absorbance with wavelength for $(C_6H_{18}N_3)[ZnCl_4]Cl$.

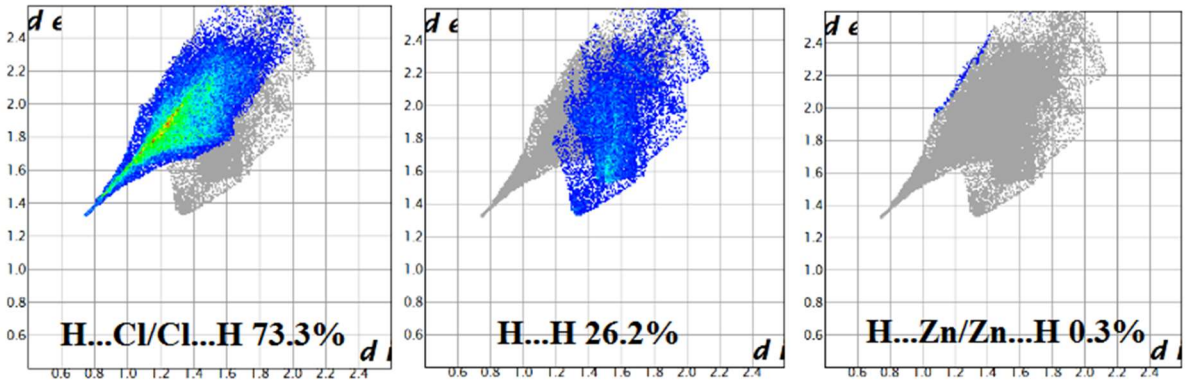

Fig. S10 2D fingerprint plots of the organic cation where areas of different intermolecular contacts are clearly shown; d_e and d_i are the distances to the nearest atom exterior and interior to the surface.

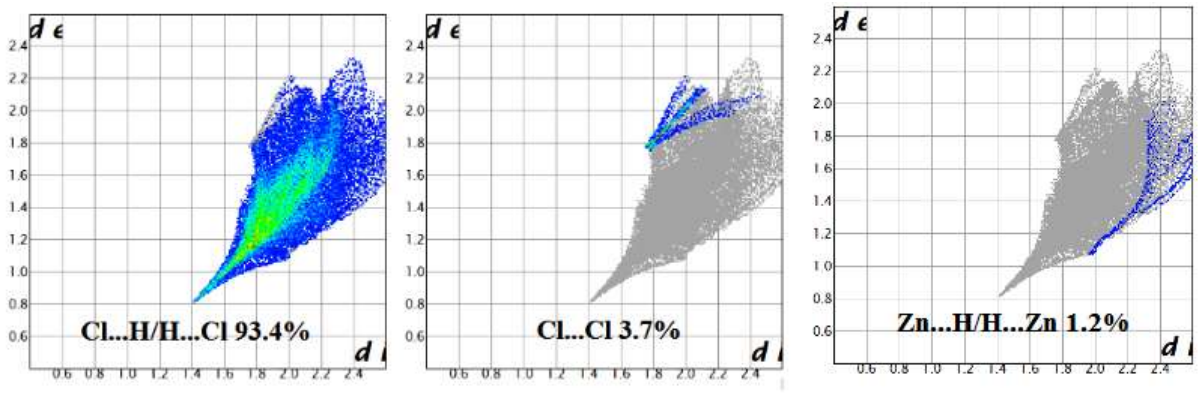

Fig. S11 2D fingerprint plots of the inorganic anion $ZnCl_4$.

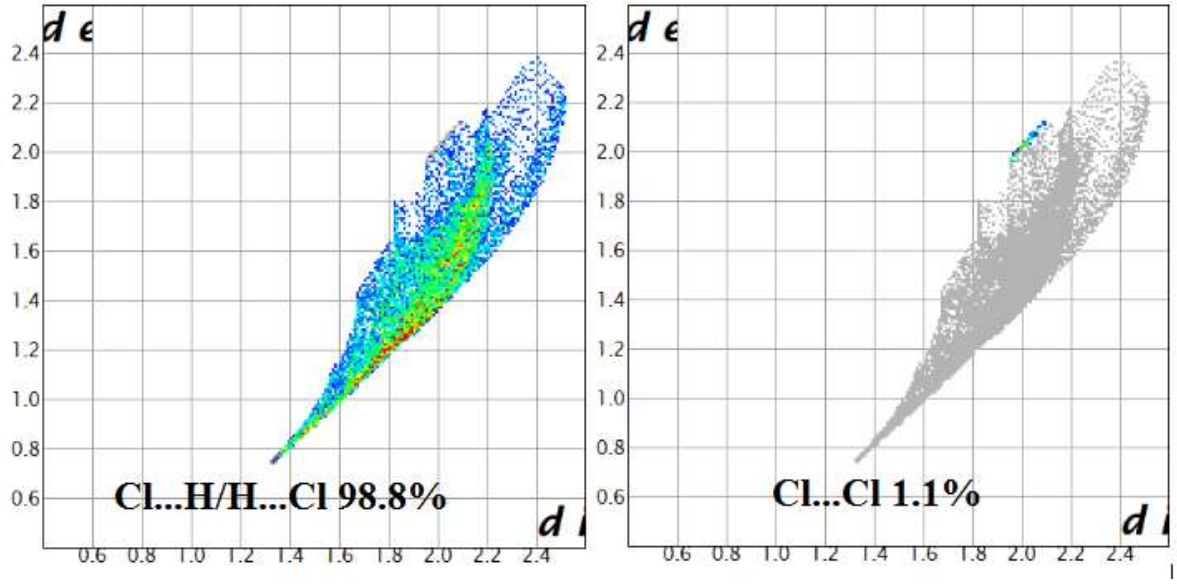

Fig. S12

2D fingerprint plots of the chloride anion.

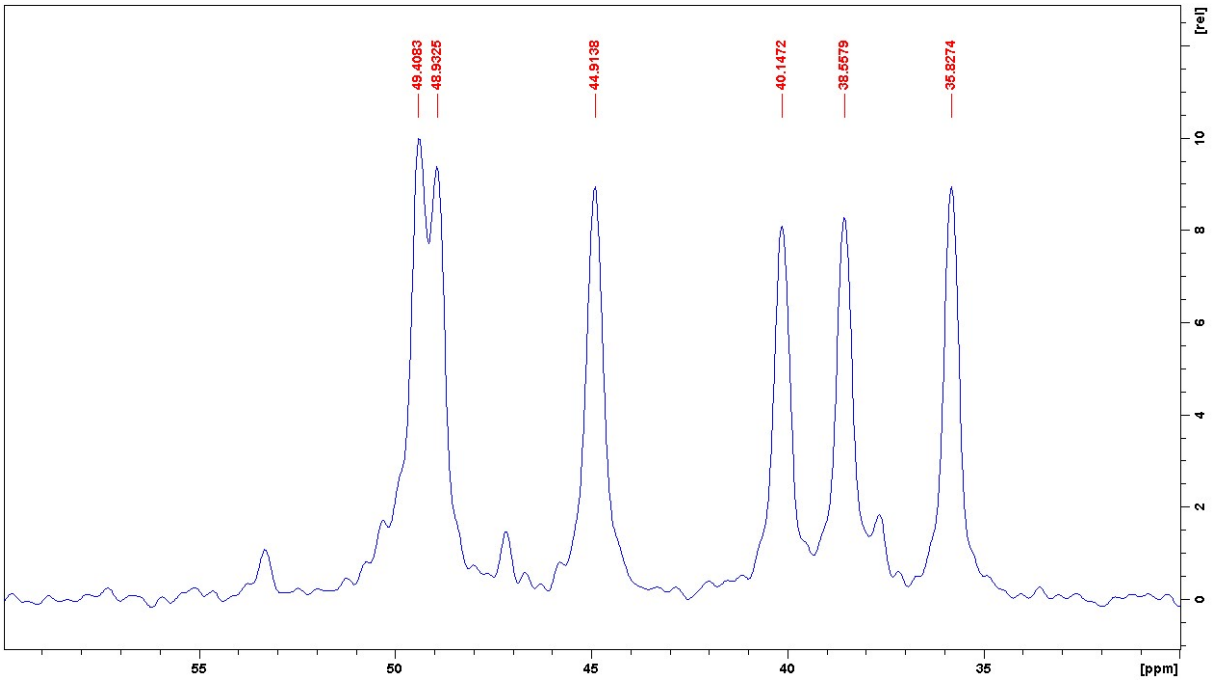

Fig. S13

^{13}C CP-MAS NMR spectrum of $(C_6H_{18}N_3)[ZnCl_4]Cl$. The small peaks in the region 20 - 40 ppm are spinning sidebands of the three peaks between 150 and 170 ppm.

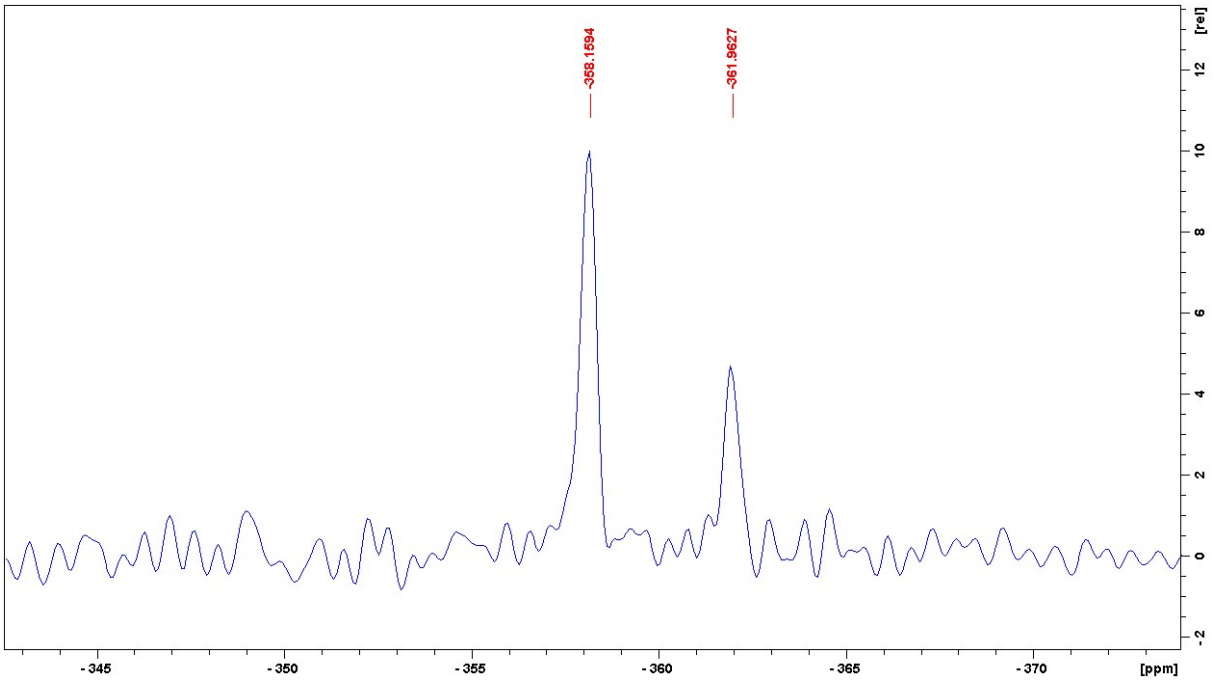

Fig. S14

^{15}N CP-MAS NMR spectrum of $(C_6H_{18}N_3)[ZnCl_4]Cl$.